JACS
JOURNAL OF THE AMERICAN CHEMICAL SOCIETY

ARTICLE

pubs.acs.org/JACS

Tunneling versus Hopping in Mixed-Valence Oligo-*p*-phenylenevinylene Polychlorinated Bis(triphenylmethyl) Radical Anions

Vega Lloveras,[†] José Vidal-Gancedo,[†] Teresa M. Figueira-Duarte,[‡] Jean-François Nierengarten,[‡] Juan J. Novoa,[§] Fernando Mota,[§] Nora Ventosa,[†] Concepció Rovira,*[,†] and Jaume Veciana*[,†]

[†]Institut de Ciència de Materials de Barcelona (CSIC) and Networking Research Center on Bioengineering, Biomaterials and Nanomedicine (CIBER-BBN), Campus Universitari de Bellaterra, E-08193 Cerdanyola, Spain

[‡]Laboratoire de Chimie des Matériaux Moléculaires, Ecole Européenne de Chimie, Polymères et Matériaux, Université de Strasbourg et CNRS (UMR 7509), 25 rue Becquerel, 67087 Strasbourg, Cedex 2, France

[§]Departament de Química Física, Facultat de Química, Universitat de Barcelona, Av. Diagonal 47, 08208 Barcelona, Spain

Supporting Information

ABSTRACT: Radical anions $\mathbf{1}^{-\bullet}$−$\mathbf{5}^{-\bullet}$, showing different lengths and incorporating up to five *p*-phenylenevinylene (PPV) bridges between two polychlorinated triphenylmethyl units, have been prepared by chemical or electrochemical reductions from the corresponding diradicals **1**−**5** which were prepared using Wittig−Horner-type chemistry. Such radical anions enabled us to study, by means of UV−vis−NIR and variable-temperature electron spin resonance spectroscopies, the long-range intramolecular electron transfer (IET) phenomena in their ground states, probing the influence of increasing the lengths of the bridges without the need of using an external bias to promote IET. The temperature dependence of the IET rate constants of mixed-valence species $\mathbf{1}^{-\bullet}$−$\mathbf{5}^{-\bullet}$ revealed the presence of two different regimes at low and high temperatures in which the mechanisms of electron tunneling via superexchange and thermally activated hopping are competing. Both mechanisms occur to different extents, depending on the sizes of the radical anions, since the lengths of the oligo-PPV bridges notably influence the tunneling efficiency and the activation energy barriers of the hopping processes, the barriers diminishing when the lengths are increased. The nature of solvents also modifies the IET rates by means of the interactions between the oligo-PPV bridges and the solvents. Finally, in the shortest compounds $\mathbf{1}^{-\bullet}$ and $\mathbf{2}^{-\bullet}$, the IET induced optically through the superexchange mechanism can also be observed by the exhibited intervalence bands, whose intensities decrease with the length of the PPV bridge.

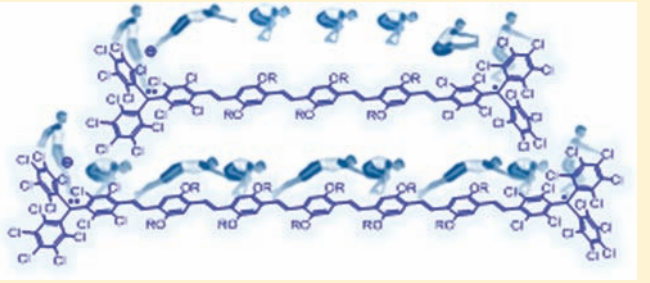

INTRODUCTION

Long-range electron transfer (ET) between donor (D) and acceptor (A) molecules/groups where the separation between the donor and acceptor greatly exceeds their spatial extent is a subject of considerable interest for studies of ET mechanisms in biological systems and in nanoscale circuits based on single molecular devices.[1−3] Electron transfer in donor−bridge−acceptor (D-B-A) molecules has been actively investigated, in part to determine which aspects of the bridge structure control the intramolecular electron transfer (IET).[4] Both the electronic structure of the bridge and the effective distance between the D/A centers are known to play a critical role in determining the ease of the ET.[4] However, very little is known about the influence of external factors, like the solvent media and temperature-induced perturbations, on the IET of nonperturbed ground states of such systems. In most of the small D-B-A systems, the ET rate scales exponentially with the length of the bridge between the D/A moieties. The distance dependence of ET rate constants, k_{ET}, is often described by $k_{ET} = k_0 \exp(-\beta d)$, where k_0 is a kinetic pre-exponential factor, d is the D−A center-to-center distance, and β is the attenuation factor that depends primarily on the nature of the molecular bridge. Theory predicts that another regime may also exist wherein the distance dependence is very weak and in which the molecular bridge essentially acts as an incoherent molecular wire, yielding a reciprocal scaling of k_{ET} with the distance.[4−11] Therefore, beyond the range of direct D−A electronic overlap, IET may occur either through a bridge-mediated superexchange — also known as direct (nonresonant) tunneling — between D/A electronic states or through an incoherent hopping. The relative contributions of these mechanisms depend in part on the electronic nature of the bridge as well

Received: September 16, 2010
Published: March 29, 2011

dx.doi.org/10.1021/ja1083859 | *J. Am. Chem. Soc.* 2011, 133, 5818–5833

Chart 1

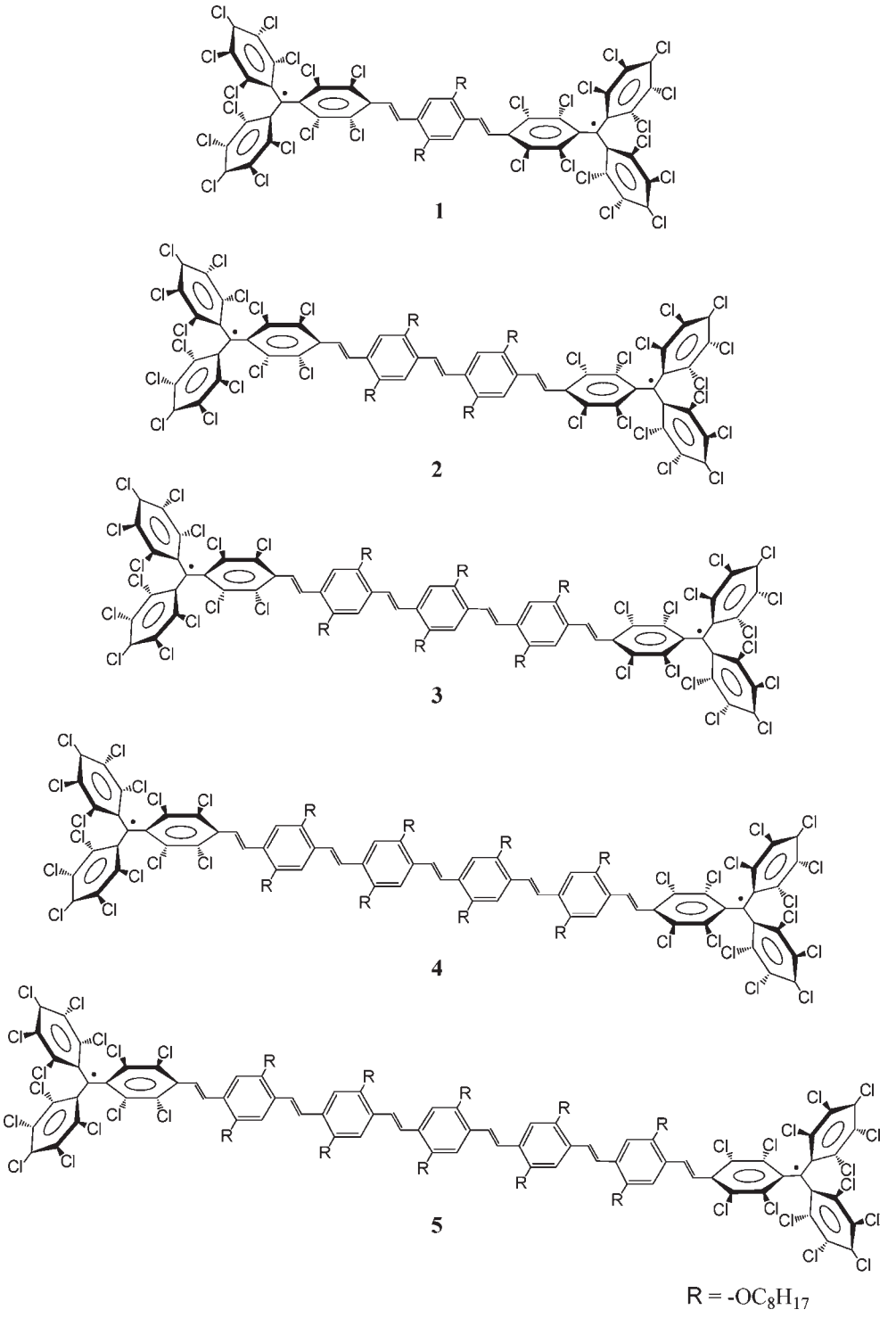

as on the distance between the D/A centers.[4] In general, tunneling and hopping pathways operate in parallel, and the overall rate constant of an IET will have contributions from both mechanisms.[12]

Mixed-valence compounds of the type R^--B-R (or R-B-R^+) containing two linked redox centers in different formal oxidation states, generated by the partial reduction (or oxidation) of symmetrical neutral R-B-R derivatives, are excellent candidates for studying the different factors influencing IETs, like the length and architectures of the bridges, as well as the temperature and the solvent. Advantageously, IET in such compounds can be studied without the need to perturb their ground states by applying an external bias using the scanning tunneling microscopy (STM) break junction technique or conducting atomic

dx.doi.org/10.1021/ja1083859 |*J. Am. Chem. Soc.* 2011, 133, 5818–5833

Scheme 1. Synthetic Route for Diradicals 1−5

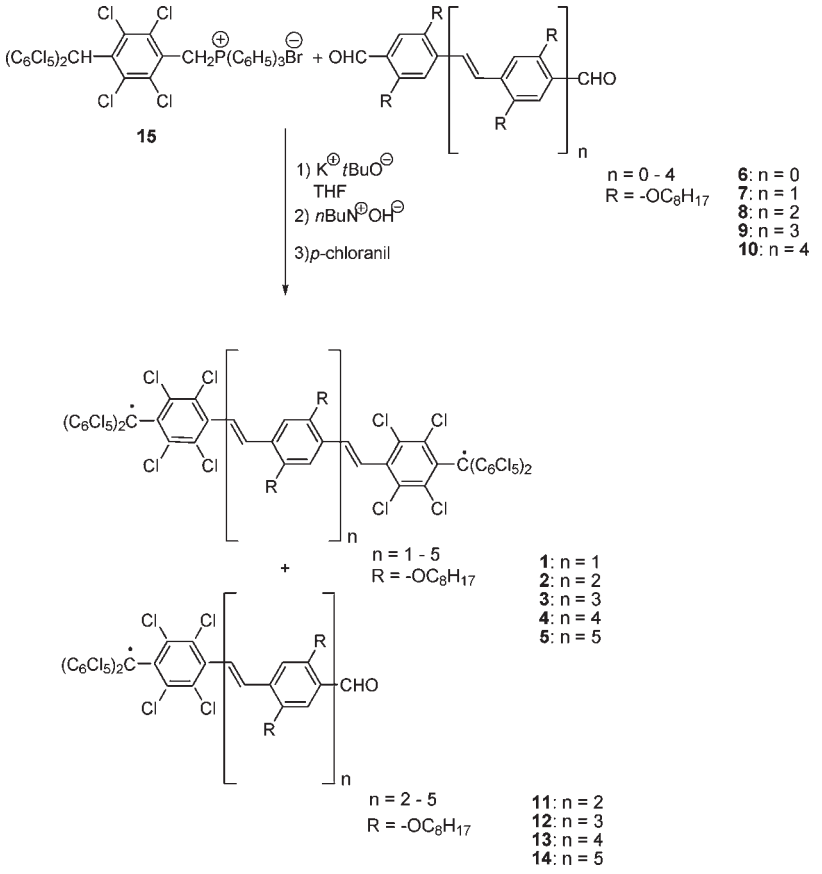

force microscopy (c-AFM), or by exciting the molecules using optical pump−probe spectroscopy.[4]

Herein, we describe a series of structurally well-defined diradicals **1**−**5** (Chart 1) in which oligo-*p*-phenylenevinylene (oligo-PPV) bridges of different lengths are connecting two polychlorotriphenylmethyl (PTM) radical units as redox centers. Such PTM radical units are particularly interesting not only because they have a large persistence, displaying high thermal and chemical stabilities, but also because they are electroactive species giving rise, either chemically or electrochemically, to the corresponding anions and cations.[13] The resulting anions are also quite stable species, while the cations are highly reactive toward H_2O, thus limiting their use.[14] By partial chemical or electrochemical reduction of diradicals **1**−**5**, we generated the mixed-valence radical anions $\mathbf{1}^{-\bullet}$−$\mathbf{5}^{-\bullet}$ and studied the optically and thermally induced IET processes from the UV−vis−NIR spectra and variable-temperature electron spin resonance (VT-ESR) spectra of these species.[15,16] The controlled molecular structure in this series of compounds allows for probing the effects of the distance on the rate at which ET occurs in these mixed-valence systems, as well as the influence of solvent and temperature on IET phenomenon and the molecular-wire behavior of the oligo-PPVs. It is worth mentioning that only a few reports on temperature control of ET through π-conjugated chains of oligo-PPVs are known.[9] Moreover, in many of those studies IETs were investigated using femtosecond to nanosecond optical pump−probe spectroscopy, where the ET takes place in the excited state, while in our study the IET is observed in the ground state.

RESULTS AND DISCUSSION

Diradicals. *Synthesis.* The synthetic route for preparing diradicals **1**−**5** is based on the reaction of phosphonium bromide **15** with the suitable oligo-PPV dialdehydes **6**−**10** under Wittig conditions followed by the *in situ* generation and oxidation of the corresponding dicarbanions with *p*-chloranil (Scheme 1).

The substituted phosphonium bromide **15**[13c] and dialdehydes **6**, **8**, and **10**[17] were prepared according to previously reported procedures. Dialdehydes **7** and **9** were obtained for the first time following the synthesis depicted in Scheme 2. The strategy employed for the preparation of such dialdehydes is based upon Wittig−Horner-type chemistry. Thus, the treatment of aldehyde **17** with phosphonate **16** in THF in the presence of *t*-BuOK afforded the targeted protected stilbene derivative **18**, but as an *E*:*Z* isomer mixture, as deduced from the ^{1}H NMR spectrum. The latter observation is quite surprising, as the reaction of benzylic phosphonates with aromatic aldehydes under Wittig−Horner conditions is generally stereoselective, leading to the *E* isomer only.[17,18] In the present case, steric hindrance resulting from the presence of the two octyloxy groups in the *ortho* positions of the reactive groups in both **16** and **17** may explain the lack of *E*:*Z* selectivity. The isomerization of the isomeric mixture to the *E* derivative **18** was easily achieved by treatment with a catalytic amount of iodine in refluxing toluene,

dx.doi.org/10.1021/ja1083859 |*J. Am. Chem. Soc.* 2011, 133, 5818–5833

Scheme 2. Synthetic Route for Obtaining Dialdehydes 7 and 9[a]

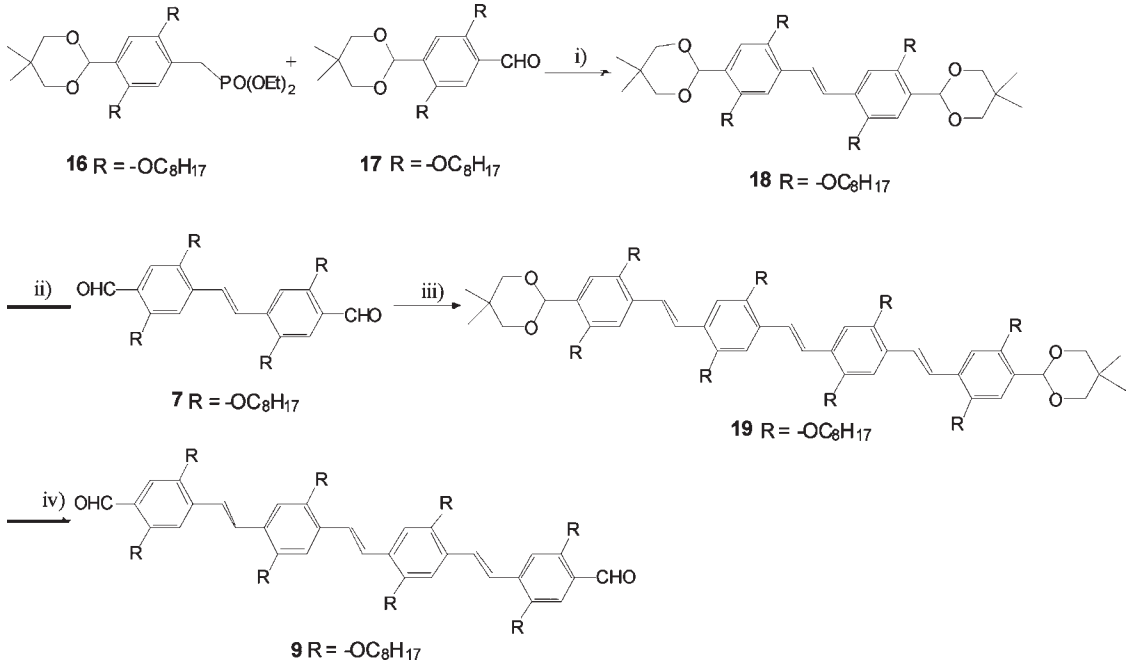

[a] Reagents and conditions: (i) *t*-BuO$^-$K$^+$/THF then I_2 (cat.)/toluene; (ii) $CF_3CO_2H/CH_2Cl_2/H_2O$; (iii) **16**/*t*-BuO$^-$K$^+$/THF then I_2 (cat.)/toluene; (iv) $CF_3CO_2H/CH_2Cl_2/H_2O$.

Chart 2

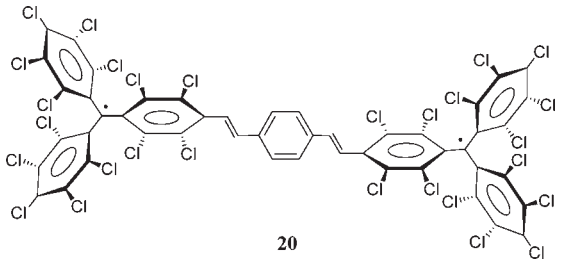

and the compound (*E*)-**18** was thus obtained in 78% yield. Subsequent deprotection with CF_3CO_2H in CH_2Cl_2/H_2O afforded the dialdehyde **7** in 74% yield. Reaction of **7** with phosphonate **16**, under Wittig−Horner conditions, followed by treatment with a catalytic amount of iodine in refluxing toluene then gave the all-*E* *p*-phenylenevinylene trimer **19** in 43% yield. Deprotection by treatment with CF_3CO_2H in CH_2Cl_2/H_2O afforded dialdehyde **9**.

The coupling of the substituted phosphonium bromide **15** with the suitable dialdehydes **6**−**10** was performed under Wittig conditions to give the corresponding polychlorinated bis(triphenylmethanes). This reaction has been strongly stereoselective in other related compounds since it yields exclusively the *E*/*E* isomers, as ascertained by NMR spectroscopy.[13c] Such stereoselectivity is justified if we consider that the ylide derived from the phosphonium bromide **15** is stabilized by the presence of the polychlorinated aromatic ring. Actually, the natural preference of ylides with electron-withdrawing groups that stabilize the betaine form has been experimentally shown to give mainly the *E* isomer.[19] In addition, the *Z*/*E* isomer distribution of the Wittig products is also strongly influenced by the nature of the base used in the preparation of the ylide.[20] Indeed, potassium *tert*-butoxide is the base of choice for maximizing the yields of *E*-olefins.[18,21]

Table 1. Redox Potentials of Compounds 1−14 in V vs Ag/$AgNO_3$ in CH_2Cl_2

compd	E^0_{red}/V	E^0_{ox1}/V
1	−0.18	1.14
2	−0.20	0.96
3	−0.22	0.86
4	−0.22	0.82
5	−0.18	0.80
6		1.79
7		1.04
8		1.03
9		0.85
10		0.80
11	−0.19	1.05
12	−0.20	0.93
13	−0.20	0.83
14	−0.18	0.78

In order to optimize the yield of the desired diradical compounds, the bis(triphenylmethane) precursors were not isolated, and the synthesis of the diradical species **1**−**5** was performed as a "one-pot" reaction by treatment of the corresponding bis(triphenylmethane) precursor with an excess of *n*-$Bu_4N^+OH^-$ and subsequent oxidation of the resulting dianions with *p*-chloranil. Apart from compound **1**, diradicals **2**−**5** were always isolated as the minor products and the corresponding radical monoadducts **11**−**14** were the major ones, whatever the reaction conditions. As already reported, the yields of Wittig-type

dx.doi.org/10.1021/ja1083859 |*J. Am. Chem. Soc.* 2011, 133, 5818–5833

Table 2. UV−Vis Data for Compounds 1−14 in CH_2Cl_2

compd	λ_{max}/nm ($10^{-3}\varepsilon/M^{-1}$ cm^{-1})			
1	321 (15.7), 368 (sh)	388 (52.3)	418 (sh)	509 (11.8), 680 (3.8)
2	338 (21.1), 368 (sh)	389 (58.1)	434 (55.3)	547 (12.2), 747 (4.9)
3	341 (27.4), 369 (sh)	390 (61.5)	454 (78.7)	558 (sh), 778 (5.7)
4	369 (sh)	389 (64.3)	462 (88.0)	579 (sh), 780 (6.2)
5	334 (34.3), 369 (sh)	389 (69.1)	475 (121.9)	585 (sh), 782 (5.9)
6	274 (16.0), 282 (13.3)		403 (6.3)	
7	331 (17.3)		423 (27.1), 476 (sh)	
8	275 (20.1), 282 (17.8), 341 (19.2)		446 (57.4)	
9	336 (19.7)		462 (67.5)	
10	333 (26.6)		470 (102.2)	
11	334 (20.9), 367 (sh)	390 (42.6)	427 (45.3)	542 (7.2), 745 (2.1)
12	339 (22.2), 368 (sh)	390 (44.2)	450 (72.1)	556 (sh), 776 (2.6)
13	333 (sh), 368 (sh)	389 (46.1)	462 (84.4)	574 (sh), 777 (2.3)
14	333 (28.1), 368 (sh)	390 (47.8)	473 (116.2)	582 (sh), 780 (2.9)

reactions involving bis-aldehydes **6**−**10** diminish drastically with the length of the conjugated system.[17] It is also worth noticing that all the obtained diradicals **1**−**5** are highly persistent and thermally stable in the solid state and also in diluted solutions, even when exposed to air. The solubility of diradicals **1**−**5** is very high in many solvents, contrasting with the behavior of the previously reported diradical **20**, lacking the two octyloxy substituents (Chart 2).[13a]

Electrochemistry. The redox properties of compounds **1**−**14** were studied in solution by cyclic voltammetry (CV) (Table 1). Cyclic voltammograms were recorded in CH_2Cl_2, with $[(n\text{-Bu})_4N]PF_6$ (0.1 M) as supporting electrolyte, a Pt wire as a working electrode, and Ag/Ag^+ as the reference electrode. Monoradicals **11**−**14** show one reversible reduction process between −0.18 and −0.20 V, corresponding to the reduction of the radical units to the corresponding monoanions. For diradicals **1**−**5**, the redox processes of the two triphenylmethyl units are too close to be distinguished, and only one reversible two-electron reduction process is observed between −0.18 and −0.22 V. This result suggests the presence of weak electronic interactions between the triphenylmethyl units of diradicals **1**−**5**, since in the case of a strong or moderate electronic interaction between the two electroactive units, two electrochemical waves are anticipated. The values of the redox potentials for the reversible reduction process of all obtained monoradicals are similar among them (see Table 1) and equal to those of the diradicals, indicating a small influence of the π-conjugation of oligo-PPV fragments on the SOMO levels of the radicals.

In oxidation, the cyclic voltammograms of monoradicals **11**−**14** and diradicals **1**−**5**, as well as those of the corresponding dialdehydes precursors **6**−**10**, exhibit from one to three reversible (or quasi-reversible) one-electron oxidation waves centered on the oligo-PPV fragments.[22] For the entire series of compounds, the first oxidation potential decreases upon increasing the conjugation length of the PPV core (Table 1).

Absorption Spectra. UV−vis absorption spectra of diradicals **1**−**5**, dialdehydes **6**−**10**, and monoradicals **11**−**14** were recorded in CH_2Cl_2, and the most relevant data are summarized in Table 2. For compounds **6**−**10**, the λ_{max} of the absorption band corresponding to the characteristic $\pi-\pi^*$ transitions of oligo-PPV units is progressively red-shifted from 403 to 470 nm when the conjugation length is increased. At the same time, the molar extinction coefficient is increased in the series, as classically observed for such systems.[22,23]

The absorption spectra of diradicals **1**−**5** (Figure 1) and monoradicals **11**−**14** also exhibit the characteristic $\pi-\pi^*$ transitions of the oligo-PPV units. In both series, this band is red-shifted upon increasing the size of the π-conjugated bridging system (Table 2). When comparing compounds **6**−**10** with the corresponding monoradicals **11**−**14**, the $\pi-\pi^*$ transitions is slightly red-shifted and the molar extinction coefficient larger. A similar trend is observed when comparing monoradicals **11**−**14** with the corresponding diradicals **1**−**5** (see Figure S1, Supporting Information). This fact is likely the result of an enhanced conjugation length of the PPV-type system due to the presence of the terminal PTM radical group. On the other hand, the presence of electronic delocalization is also observed in the two low-energy radical bands that appear around 509−585 and 680−782 nm, in which bathochromic shifts and enhanced absorptivities cause the conjugation of the oligo-PPV bridges to increase. As previously noted, increasing the number of PPV fragments in the monoradicals also gives rise to small red shifts and enhanced absorptivities of these bands, although to a lesser extent than in the diradicals.

It is worth mentioning that the changes in these low-energy bands of the diradicals are much more pronounced when going from diradical **1** to **3** than from **3** to **5**. Such low-energy radical bands are assigned to charge transfer from the electron-donating PPV bridge to the electron-accepting PTM radical groups. This assignment is confirmed by the absence of such absorptions in the corresponding dianionic species generated from the radicals (*vide infra*), where the acceptor character of PTM units is absent, and is also supported by the solvent dependence shift, typical of charge-transfer bands, exhibited by the low-energy radical bands of diradical **1**. On the other hand, the most characteristic radical absorption, attributable to the HOMO−SOMO transition,[24] appears in all radicals at 389 nm without showing any significant difference with the size of the bridging conjugated system.

Electron Spin Resonance. X-band ESR spectra of diradicals **1**−**5** and monoradicals **11**−**14** were recorded in CH_2Cl_2/toluene (1:1) solution in the temperature range of 140−300 K. In both cases, the ESR spectra at 300 K are practically identical along the series (Table 3). As representative examples, the experimental and simulated spectra of diradical **3** and monoradical **12** are shown in Figures 2 and 3, respectively.

dx.doi.org/10.1021/ja1083859 |*J. Am. Chem. Soc.* 2011, 133, 5818–5833

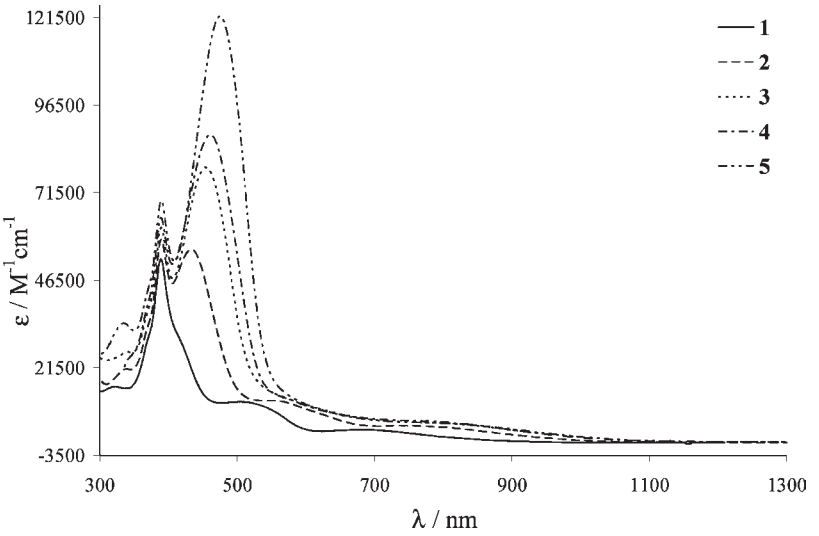

Figure 1. UV−vis spectra of diradicals **1**−**5** in CH_2Cl_2.

Table 3. EPR Data[a] for Diradicals 1−5 and Monoradicals 11−14 Obtained in CH_2Cl_2/Toluene (1:1) Solution

compd	T/K	g	a_H	$a_{C,\alpha}$	$a_{C,arom}$	ΔH_{pp}
1	220	2.0025	0.88 (2 H)	14.8	6.5, 5.4	0.88[b]
2	220	2.0022	0.88 (2 H), 0.34 (2 H)	14.5	6.2, 5.1	0.32
3	220	2.0022	0.93 (2 H), 0.36 (2 H)	14.6	6.2, 5.1	0.36
4	220	2.0024	0.87 (2 H), 0.37 (2 H)	14.1	6.2, 5.3	0.40
5	230	2.0023	0.90 (2 H), 0.38 (2 H)	13.6	6.2, 5.4	0.40
11	220	2.0020	1.80 (1 H), 0.70 (1 H)	29.1	12.7, 10.2	0.56
12	220	2.0022	1.75 (1 H), 0.70 (1 H)	28.9	12.7, 10.2	0.62
13	220	2.0022	1.80 (1 H), 0.70 (1 H)	29.0	12.5, 10.1	0.65
14	240	2.0023	1.80 (1 H), 0.70 (1 H)	29.3	12.5, 10.2	0.69
$\mathbf{1}^{-\bullet}$	200	2.0025	1.70 (1 H)			1.0
$\mathbf{2}^{-\bullet}$	205	2.0022	1.65 (1 H), 0.72 (1 H)			0.85
$\mathbf{3}^{-\bullet}$	220	2.0024	1.70 (1 H), 0.70 (1 H)			0.70
$\mathbf{4}^{-\bullet}$	220	2.0024	1.68 (1 H), 0.72 (1 H)			0.80
$\mathbf{5}^{-\bullet}$	240	2.0023	1.70 (1 H), 0.70 (1 H)			0.80

[a] *g*, Lande factor (±0.0003); a_X, hyperfine coupling constant (in gauss) with atom X; ΔH_{pp}, peak-to-peak line width (in gauss). [b] The larger line width of **1** is ascribed to the larger dipolar interaction in this diradical.

At 300 K, monoradicals showed ESR spectra with two symmetrical main lines originated by the hyperfine coupling of the unpaired electron with the hydrogen atom of the ethylene group next to the PTM unit. Several weak satellite lines corresponding to the hyperfine couplings with the naturally abundant ^{13}C nuclei of the PTM unit (Table 3) were also observed. When the temperature was lowered, the main lines narrowed, thus making it possible to distinguish an additional hyperfine coupling with another hydrogen atom of the ethylene moiety, with a smaller hyperfine coupling constant, yielding a spectrum consisting of four main lines (see Figure 3b and Table 3). Spectra of diradicals **1**−**5** at 300 K are different since they exhibit three overlapped symmetrical main lines, which are each split into two lines when the temperature is lowered (see Figure 2b), with isotropic hyperfine coupling constants that are approximately half those of the monoradicals. The ^{13}C hyperfine coupling constants in the biradicals are also half the values of the coupling constants of monoradicals. As the isotropic hyperfine coupling constants for diradicals **1**−**5** are half those found for the related monoradicals **11**−**14** (see Table 3), we can conclude that the two electrons in diradicals **1**−**5** are magnetically interacting, with an electron exchange interaction constant, *J*, that fulfills the condition $|J| \gg |a_i|$.[25] The isotropic g_{iso} values for all studied mono- and diradicals are very close to that of the free electron (Table 3), as already observed for other substituted PTM radicals.[13,14]

Spectra of diradicals were also recorded in a frozen CH_2Cl_2/toluene (1:1) mixture at 140 K in order to determine the absolute values of zero-field-splitting parameters, $|D/hc|$ and $|E/hc|$, that arise from the dipolar magnetic interactions between the two unpaired electrons. The values of these parameters for diradical **1** are $|D/hc| = 3.9 \times 10^{-4}$ cm^{-1} (or $D = 8.5$ G) and $|E/hc| \approx 0$, which are equal to those of diradical **20**, lacking the two octyloxy substituents.[26] Such an agreement reveals a similar dipolar magnetic interaction between the two unpaired electrons of both diradicals and a weak influence of the two electron-withdrawing octyloxy susbtituents of the central phenyl ring on the distribution of the two unpaired electrons. From the zero-field-splitting parameter $|D/hc|$, one may also estimate an effective interspin separation, *R*, assuming that $D = 3g^2\beta^2/2R^3$,[26−28] strictly valid only for localized diradicals, is applicable to the delocalized diradicals studied here. Indeed, one may estimate an effective distance of 15 Å for diradical **1**, which is somewhat smaller than the nominal separation of 18.8 Å between the two methyl carbon atoms calculated from optimized structures using AM1 semiempirical minimizations. This result is in agreement with a certain degree of electronic delocalization for **1**. For the rest of diradicals (**2**−**5**), their *D* values are either very small ($D \leq 1$ G) or undetectable by conventional continuous-wave ESR, as expected from the large distances between the two methyl carbon atoms, estimated by theoretical calculations as 18.8, 25.4, 31.9, 38.2, and 44.7 Å for **1**−**5**, respectively.[28] In line with such large distances is the fact that any of the forbidden $\Delta M_s = 2$ transitions were observed for the studied diradicals at half-field in the ESR spectra at 140 K.

Radical Anions. *Generation of Radical Anions.* Mixed-valence radical anions $\mathbf{1}^{-\bullet}$−$\mathbf{5}^{-\bullet}$were generated by the chemical reduction of diradicals **1**−**5** with metallic Cu under conditions

dx.doi.org/10.1021/ja1083859 |*J. Am. Chem. Soc.* 2011, 133, 5818–5833

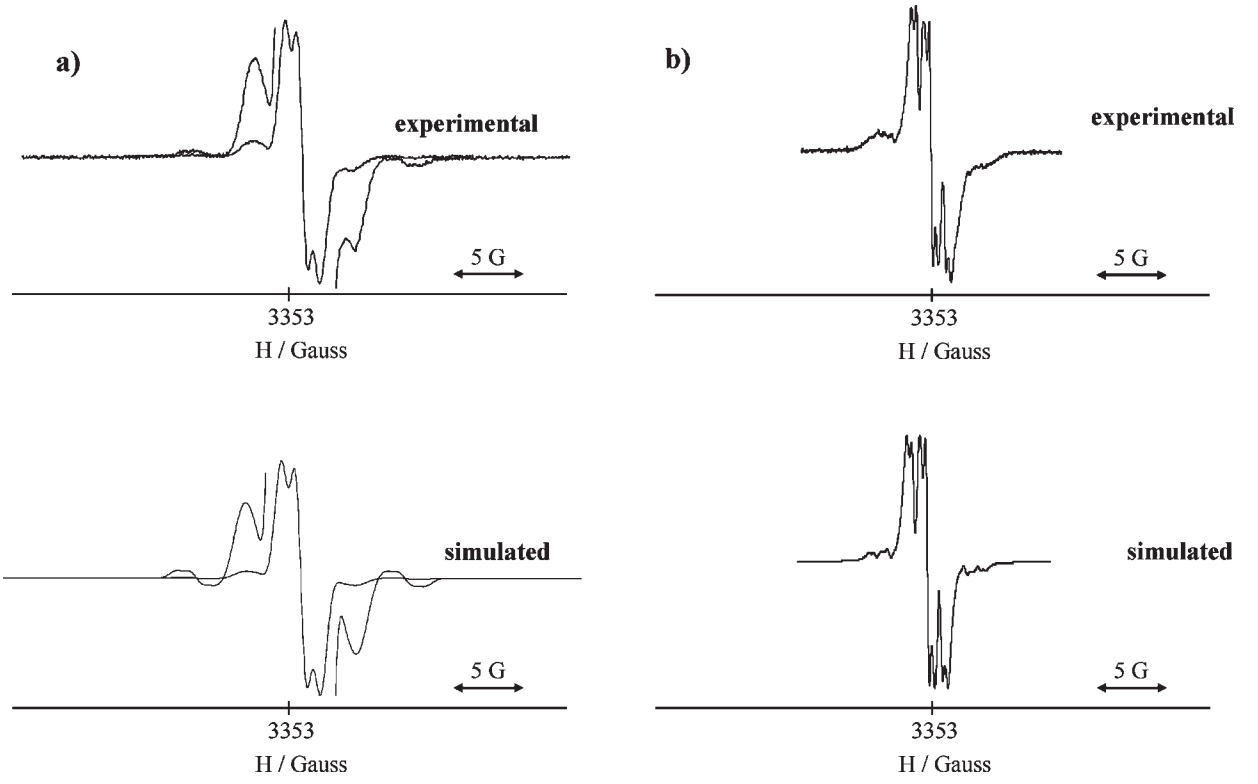

Figure 2. Experimental and simulated isotropic solution EPR spectra of diradical **3** in CH_2Cl_2/toluene (1:1) solution at 300 (a) and 220 K (b).

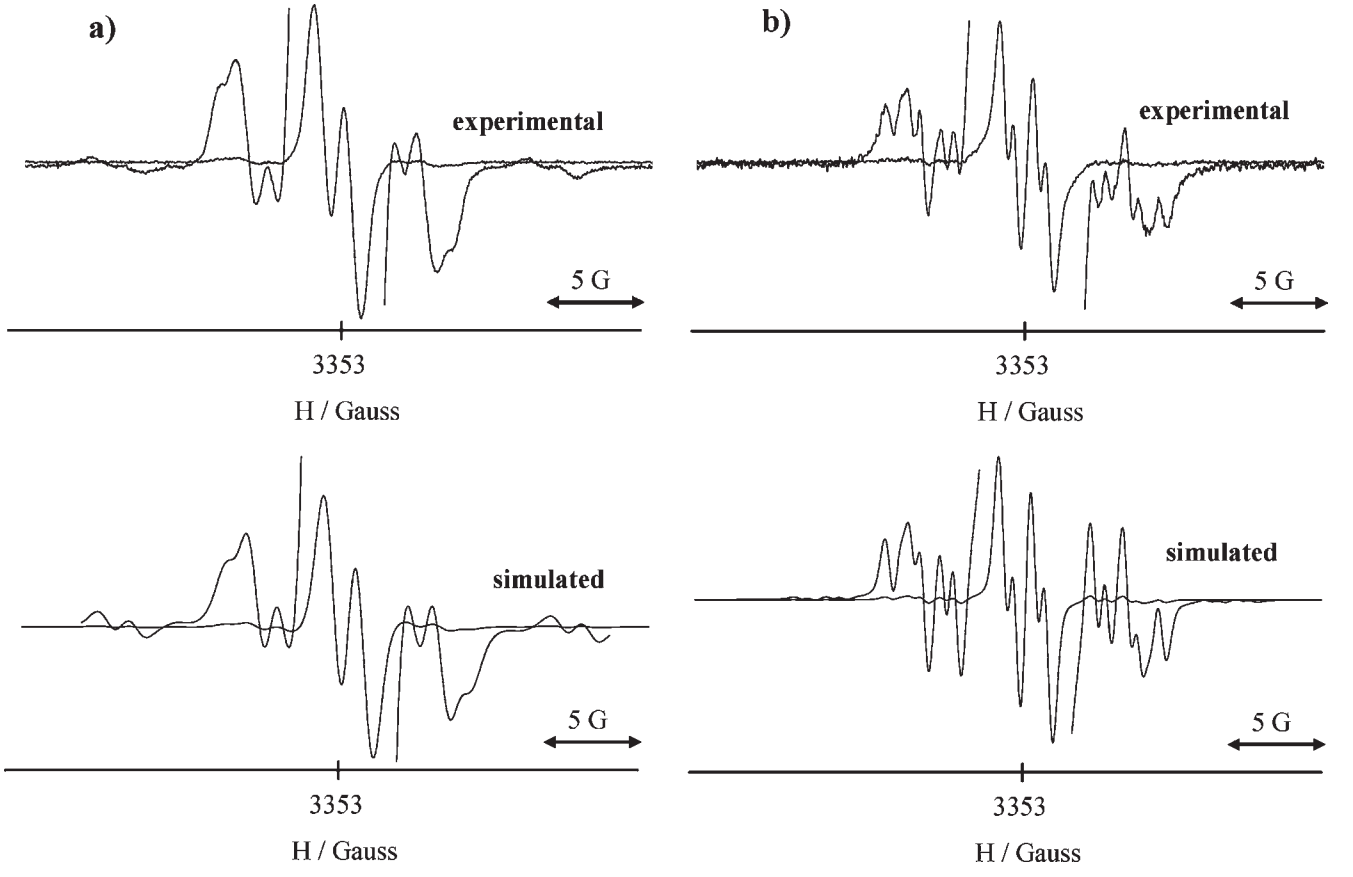

Figure 3. Experimental and simulated isotropic solution EPR spectra of monoradical **12** in CH_2Cl_2/toluene (1:1) solution at 300 (a) and 220 K (b).

dx.doi.org/10.1021/ja1083859 |*J. Am. Chem. Soc.* 2011, 133, 5818–5833

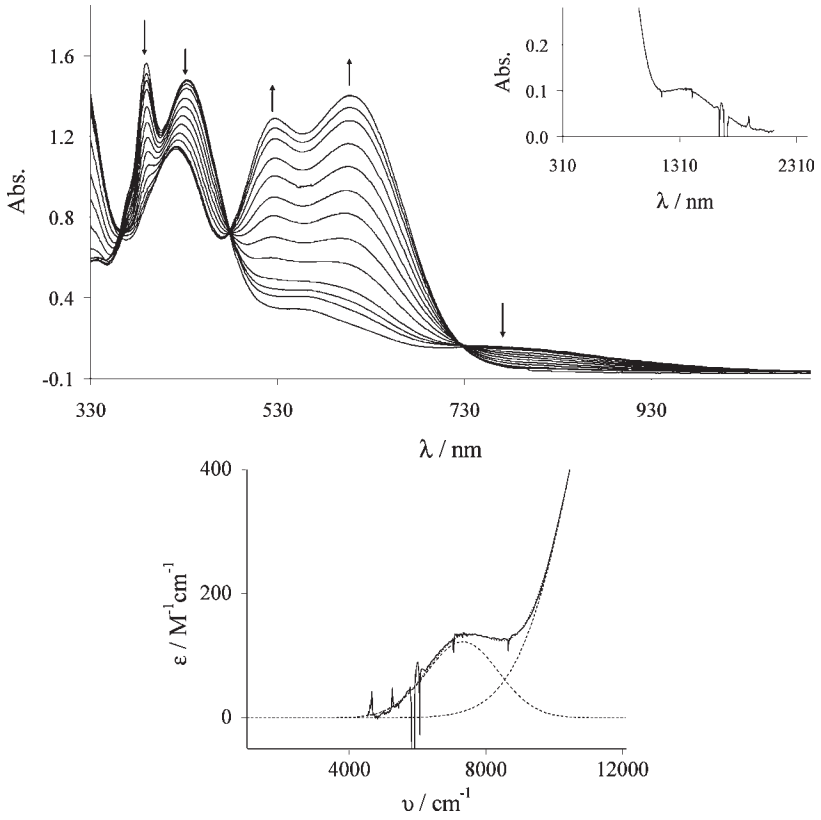

Figure 4. Top: Evolution of the UV−vis during the course of the reduction of diradical **2** in CH_2Cl_2 with metallic Cu. Inset shows the intervalence band at the NIR region of radical anion $\mathbf{2}^{-\bullet}$. Bottom: Experimental intervalence band (solid line) of $\mathbf{2}^{-\bullet}$, which was deconvoluted by means of two Gaussian functions (dashed lines). Notice that the sum of the dashed lines (dotted line) closely matches the experimental spectrum.

previously optimized for the reduction of (2,3)-(6,7)-bis(1,4-dioxo-1,4-dihydrobenzo)tetrathiafulvalene.[16d,27] Thus, the reduction was performed on stirred 1×10^{-4}−2.5×10^{-4} M solutions of **1**−**5** in CH_2Cl_2 with $[(Ph)_4P]$ Br (0.1 M) as supporting electrolyte and using a wire of metallic copper as the reducing chemical agent. This process takes place smoothly and gradually, and it can be stopped at any point just by removing the copper wire from the solution. The reduction progress was followed continuously by UV−vis−NIR spectroscopy until the dianions were fully generated. As an example, Figure 4 illustrates the evolution of the absorption spectra during the course of the reduction of diradical **2**, where the formation of the radical anion $\mathbf{2}^{-\bullet}$ followed by the dianion $\mathbf{2}^{2-}$ is observed. The observation of some well-defined isosbestic points during the course of the reduction indicates that no byproducts due to decompositions are originated during this smooth process. For comparison purposes, the monoanions $\mathbf{11}^{-}$−$\mathbf{14}^{-}$ were also generated from the radicals **11**−**14** using the same reduction procedure. All relevant spectroscopic data of the final products — the dianions $\mathbf{1}^{2-}$−$\mathbf{5}^{2-}$ and monoanions $\mathbf{11}^{-}$−$\mathbf{14}^{-}$ — are collected in Table 4.

In all reduction reactions of radicals, the initial band centered around 389 nm, characteristic of the PTM radical chromophore, decreases until it disappears completely when all radical centers are reduced to anions. Also the least energetic band of the mono- and diradicals, centered between 680 and 782 nm, completely disappears when the corresponding anions are formed. The last observation supports the assignment of this band to charge-transfer absorption from the PPV electron-donor fragment to the PTM electron-acceptor units. In all the resulting mono- and dianions, the absorption bands

Table 4. UV−Vis Data for Anions $\mathbf{1}^{2-}$−$\mathbf{5}^{2-}$ and $\mathbf{11}^{-}$−$\mathbf{14}^{-}$ in CH_2Cl_2 with $[(Ph)_4P]Br$ (0.1 M)

compd	λ_{max}/nm ($10^{-3}\varepsilon$/M^{-1} cm^{-1})		
$\mathbf{1}^{2-}$		525 (44.3)	612 (45.9)
$\mathbf{2}^{2-}$	421 (42.5)	526 (48.0)	609 (52.4)
$\mathbf{3}^{2-}$	445 (69.6)	526 (53.8)	606 (56.9)
$\mathbf{4}^{2-}$	457 (79.0)	526 (57.1)	604 (58.2)
$\mathbf{5}^{2-}$	473 (115.8)		602 (66.2)
$\mathbf{11}^{-}$	421 (38.2)	525 (27.8)	606 (28.3)
$\mathbf{12}^{-}$	447 (65.7)	525 (31.4)	603 (31.9)
$\mathbf{13}^{-}$	459 (78.1)	525 (32.3)	601 (33.6)
$\mathbf{14}^{-}$	472 (111.3)		599 (36.0)

produced by the oligo-PPV moieties are blue-shifted with respect to those exhibited by the neutral radicals and their intensity decreases, showing that, in the mono- and dianions, the π-conjugation of the PPV-type moiety is less extended than in their corresponding radicals.

The mono- and dianions show two new broad and intense bands between 525 and 612 nm, one of which always appears centered at 525 nm in all mono- and dianions, while the least energetic one is blue-shifted from 612 to 602 nm when going from $\mathbf{1}^{2-}$ to $\mathbf{5}^{2-}$. In the largest anionic species $\mathbf{14}^{-}$ and $\mathbf{5}^{2-}$, both with five PPV units, only the least energetic band was observed since the other band is probably inside the intense band generated by the PPV moiety.

Optically Induced Intramolecular Electron Transfer in $\boldsymbol{1}^{-\bullet}$−$\boldsymbol{5}^{-\bullet}$. During the reduction of diradicals **1** and **2**, together with the above-described absorptions, a weak and broad band appears in the NIR region (see Figure 4 inset) whose intensity

dx.doi.org/10.1021/ja1083859 |*J. Am. Chem. Soc.* 2011, 133, 5818–5833

Table 5. IVT Absorption Data of $1^{-\bullet}$, $2^{-\bullet}$, and $20^{-\bullet}$, Acquired Using Chemical Reduction with Cu in CH_2Cl_2 with $[(Ph)_4P]Br$ (0.1 M), along with the Effective Electronic Couplings and Separations of the Two Redox Sites

compd[a]	ν_{max}/cm^{-1}	$\varepsilon_{max}/M^{-1}\,cm^{-1}$	$\Delta\bar{\nu}_{1/2}/cm^{-1}$	R/Å	V_{ab}/cm^{-1}
$1^{-\bullet}$	7090	451	3150	18.8	109
$2^{-\bullet}$	7553	264	2110	25.4	52
$20^{-\bullet}$	6349	677	2940	18.8	123

[a] Data for $20^{-\bullet}$ were taken from ref 13c.

increases until a complete formation of the mixed-valence radical anion species $1^{-\bullet}$ and $2^{-\bullet}$ is achieved. From that point the intensity of this band decreases as the radical anion is progressively transformed into the dianion. This optical transition is expected for mixed-valence compounds that belong to Robin and Day's class II[28] in which an optically induced IET phenomenon, produced by a bridge-mediated superexchange (tunneling) mechanism, takes place. For such optical transitions, when the distance between the two electroactive centers increases, the intensity of the intervalence transition (IVT) band decreases and at the same time is shifted toward shorter wavelengths, as is indeed observed for $1^{-\bullet}$ and $2^{-\bullet}$, which show IVT bands at 1420 and 1380 nm, respectively. For the mixed-valence species $3^{-\bullet}$, $4^{-\bullet}$, and $5^{-\bullet}$, no IVT bands were observed, even after a careful deconvolution of their spectra. This result is not surprising because the calculated distances between the two methyl carbon atoms are too large to detect any IVT band.[29] In fact, IVT bands are increasingly difficult to detect when the distance between the two redox centers approaches 20−25 Å because of the exponential decay of its intensity.[4] As a rule of thumb, the tunneling is not effective over distances greater than ∼25 Å.[30]

In order to determine the effective electronic coupling, V_{ab}, between the two equivalent electroactive centers of radical anions $1^{-\bullet}$ and $2^{-\bullet}$, we applied the equation developed by Hush,[31] as was previously done for the radical anion $20^{-\bullet}$.[13,26]

$$V_{ab} = [2.05 \times 10^{-2}\sqrt{\varepsilon_{max}\bar{\nu}_{max}\Delta\bar{\nu}_{1/2}}]R \qquad (1)$$

Here, V_{ab} is the tunneling matrix element (in cm^{-1}), ε_{max} the maximum extinction coefficient (in $M^{-1}\,cm^{-1}$), $\bar{\nu}_{max}$ the transition energy (in cm^{-1}), $\Delta\bar{\nu}_{1/2}$ the full-width at half-height (in cm^{-1}) of the IVT band, and R the effective separation of the two redox sites (in Å), which can be estimated from semiempirical calculations. The resulting data, shown in Table 5, were obtained after correction for the comproportionation equilibrium and by deconvolution of the experimental spectra (see Figure 4).

The effective electronic coupling values obtained for the mixed-valence species $1^{-\bullet}$ and $2^{-\bullet}$ are 109 and 52 cm^{-1}, respectively, showing a large decrease of the tunneling matrix element as the effective distance between the redox sites increases. This is the normal behavior expected for a tunneling mechanism, mediated by superexchange through the bridge, whose intensity decreases exponentially with the distance between the centers. On the other hand, the V_{ab} value for $1^{-\bullet}$ is somewhat lower than that previously reported for the nonsubstituted related radical anion $20^{-\bullet}$.[26] This result suggests that steric and electronic effects of the two octyloxy substituents on the six-member ring slightly influence on the effective electronic coupling. Probably steric hindrance between the bulky octyloxyl substituents and the chlorine atoms on the neighboring phenyl rings of PTM units is at the origin of a loss of coplanarity among the bridge and the PTM units (*vide infra*) and, consequently, a slight decrease of the effective electronic coupling between the terminal sites.

Thermally Induced Intramolecular Electron Transfer in $1^{-\bullet}$*−*$5^{-\bullet}$. We also studied the thermally activated IET process in $1^{-\bullet}$*−*$5^{-\bullet}$ by means of VT-ESR spectroscopy. For this purpose, the electrochemical reduction of diradicals **1**−**5** was performed until an almost complete reduction to 1^{2-}*−*5^{2-} was achieved. This procedure is advantageous since it avoids interferences from the diradical precursors and the resulting solutions contain, besides a small concentration of the desired mixed-valence $1^{-\bullet}$*−*$5^{-\bullet}$ species, a large concentration of the ESR-silent 1^{2-}*−*5^{2-} species, thereby providing good spectral resolutions.

The ESR data of all radical anions $1^{-\bullet}$*−*$5^{-\bullet}$ in CH_2Cl_2 at low temperatures are gathered in Table 3. All compounds display four main lines at low temperature in their ESR spectra, which are very similar to those of the related monoradicals **11**−**14** (see Table 3). These characteristics are consistent with the coupling of the unpaired electron of these species with the two hydrogen atoms of the ethylene moiety directly linked to the PTM radical unit, showing at the same time that these radical anions are at the "slow-exchange" regime under such conditions. By contrast, at room temperature and at intermediate temperatures, the spectral features differ notably from those observed at low temperature, indicating that a dynamic IET takes place on the ESR time scale.

To perform a complete VT-ESR study with compounds $1^{-\bullet}$*−*$5^{-\bullet}$, we selected CH_2Cl_2 and 1,2-dichlorobenzene as the solvents of choice because both solvents solubilize all radical anions, as well as the electrolyte in which they are generated, and both have low dielectric constants, enabling ESR spectra to be obtained with good resolution. In addition, the melting and boiling points of both solvents are very different, ensuring a large temperature range for variable-temperature measurements. Thus, the VT-ESR study in CH_2Cl_2 in the temperature range of 200−310 K allowed us to follow completely the IET processes in $1^{-\bullet}$, $2^{-\bullet}$, and $3^{-\bullet}$. As an example, we show in Figure 5 the VT-ESR spectra of the mixed-valence species $2^{-\bullet}$ (see also Figure S2). The ESR spectrum of this radical anion at 200 K displays two symmetrical lines arising from the hyperfine coupling with only one hydrogen atom of the ethylene moiety. This result demonstrates that, at this temperature, the unpaired electron of radical anion $2^{-\bullet}$ is localized on only one half of the molecule on the ESR time scale, being therefore at the "slow-exchange" regime. When the temperature increases, a new central line gradually emerges between the two initial ones. This evolution is consistent with the increase of the IET rate between the two sites going from the "slow-exchange" limit at 200 K to the "fast-exchange" regime at 300 K. In the latter region the unpaired electron of $2^{-\bullet}$ is coupled with two ^1H nuclei of both ethylene groups, both becoming equivalent nuclei due to the high rate of the ET. The resulting spectrum displays three main lines with a hyperfine coupling constant half the value of that at low temperature. The simulation of ESR spectra[32] at different temperatures yielded the IET rate constants, k_{ET}, that vary from $8.1 \times 10^6\ s^{-1}$ at 200 K to $2.1 \times 10^8\ s^{-1}$ at 310 K (Figure 5). On going from $1^{-\bullet}$ to $3^{-\bullet}$, the rate constants k_{ET} at a given temperature decrease, indicating that the IET process is slowed as the distance between the electroactive centers increases. In accordance, species $4^{-\bullet}$ and $5^{-\bullet}$, with even larger bridges, appear as totally localized species in the range of temperatures allowed by CH_2Cl_2.

The shape evolution trend with temperature of the ESR spectra of anion radicals $1^{-\bullet}$*−*$5^{-\bullet}$ in 1,2-dichlorobenzene was

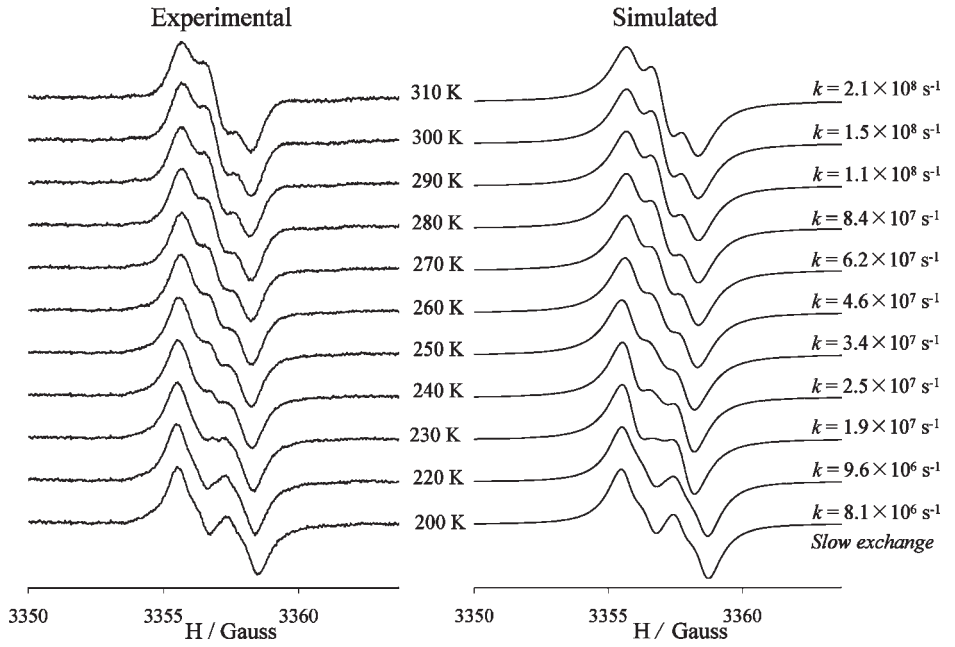

Figure 5. VT-ESR spectra of $\mathbf{2}^{-\bullet}$ in CH_2Cl_2 with 0.1 M of $[(Ph)_4P]Br$. Experimental spectra in the temperature range of 200−310 K (left) and simulated spectra (right) with different IET rates.

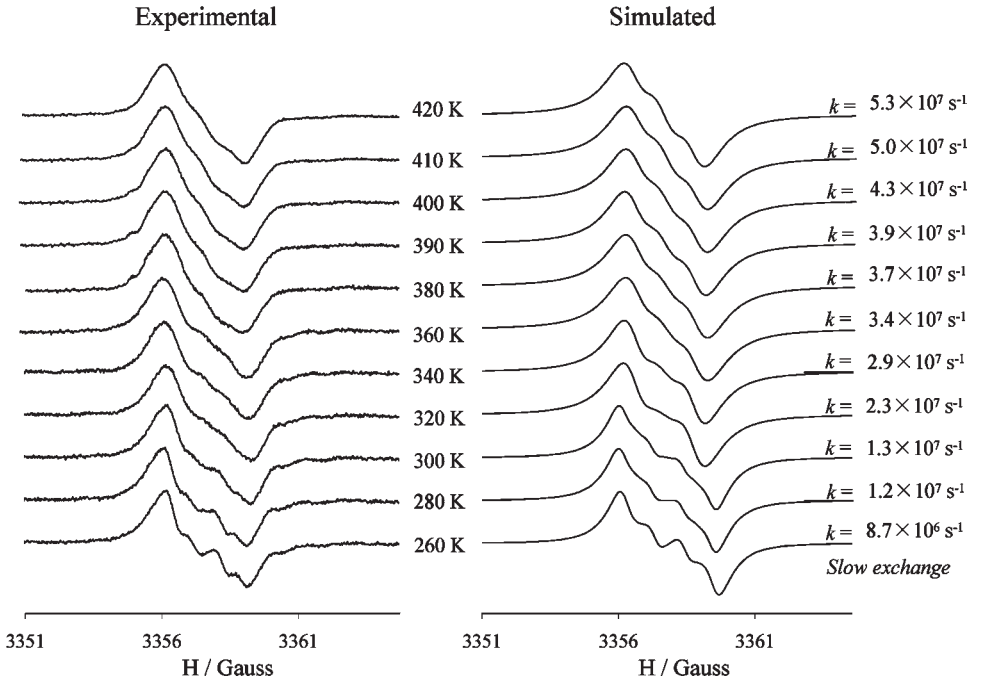

Figure 6. VT-ESR spectra of $\mathbf{4}^{-\bullet}$ in 1,2-dichlorobenzene with 0.1 M $[(Ph)_4P]Br$. Experimental spectra in the temperature range of 260−420 K (left) and simulated spectra (right) with different IET rates.

similar to that obtained in CH_2Cl_2 (see Figures 6, S3, and S4). Nevertheless, in this case it was possible to record spectra at very elevated temperatures and accordingly to follow IET processes with higher rate constants. As an example, for compound $\mathbf{1}^{-\bullet}$, CH_2Cl_2 allowed a maximum rate of only $6.3 \times 10^8\ s^{-1}$, while with 1,2-dichlorobenzene the maximum rate was $10.0 \times 10^8\ s^{-1}$. 1,2-Dichlorobenzene also made it possible to follow the thermally activated IET process of the mixed-valence species $\mathbf{4}^{-\bullet}$ (Figure 6) and to observe a small change in the IET rate constants of the mixed-valence species $\mathbf{5}^{-\bullet}$ on going from 300 to 420 K (see Figure S4), because this compound is at the "slow- exchange" regime below 300 K. Experimental ESR spectra of all five mixed-valence species at 320 K in 1,2-dichlorobenzene (see Figure S5) clearly demonstrate that the rate constants decrease with the oligo-PPV bridge lengths.

dx.doi.org/10.1021/ja1083859 |*J. Am. Chem. Soc.* 2011, 133, 5818–5833

In order to understand the IET mechanism operating in anion radicals $\mathbf{1}^{-\bullet}-\mathbf{5}^{-\bullet}$, we studied the temperature dependence of the k_{ET} values obtained from the simulation of the VT-ESR spectra of $\mathbf{1}^{-\bullet}-\mathbf{3}^{-\bullet}$ in CH_2Cl_2 and $\mathbf{1}^{-\bullet}-\mathbf{4}^{-\bullet}$ in 1,2-dichlorobenzene. Unfortunately, the lack of experimental data available for $\mathbf{5}^{-\bullet}$, even in 1,2-dichlorobenzene, prevented its inclusion in this study. As already mentioned, in mixed-valence systems the IET may occur either through a bridge-mediated superexchange (or direct tunneling) process between donor and acceptor electronic states or through an incoherent hopping process; both mechanisms can operate in parallel, with the overall rate constant receiving contributions from both mechanisms.[12] The temperature dependences of the two pathways can be used to clarify the relative importance of each, since the tunneling mechanism in principle should not be dependent on temperature, while the hopping process must follow a classical Arrhenius relation. The Arrhenius plots $\log(k_{ET})$ vs $1/T$ of the k_{ET} values obtained from the VT-ESR spectra for $\mathbf{1}^{-\bullet}-\mathbf{3}^{-\bullet}$ in CH_2Cl_2 and for $\mathbf{1}^{-\bullet}-\mathbf{4}^{-\bullet}$ in 1,2-dichlorobenzene are depicted in Figure 7, and the associated kinetic data, such as the activation energy barriers, E_a, and exponential prefactors, A, are gathered in Table 6. The Arrhenius plots in CH_2Cl_2 can be separated into two distinct temperature regions: the low-T region at $T < 240$ K for $\mathbf{1}^{-\bullet}$, <270 K for $\mathbf{2}^{-\bullet}$, and <280 K for $\mathbf{3}^{-\bullet}$, and the high-T region at higher temperatures. In the latter region there is a stronger temperature dependence with larger slopes, which suggests a dominant thermally activated hopping process. In this region, the activation energy barriers and the exponential prefactors decrease as the length of the bridges increases (Table 6). In the low-T region the three radical anions exhibit lower values for both E_a and A parameters than in the high-T regime. Arrhenius plots with VT-ESR data of $\mathbf{1}^{-\bullet}$ and $\mathbf{2}^{-\bullet}$ in 1,2-dichlorobenzene also show the existence of two distinct temperature regimes (Figure 7, bottom), while the two regimes are not distinguished for $\mathbf{3}^{-\bullet}$ and $\mathbf{4}^{-\bullet}$, indicating the existence of only the high-T one. In the latter regime the E_a and A values for $\mathbf{1}^{-\bullet}-\mathbf{4}^{-\bullet}$ also decrease as the length of the bridge increases (Table 6).

The presence of two temperature regions in both solvents could be explained in two alternative ways: (a) the existence of two parallel conventional thermally activated IET processes with different kinetic parameters A and E_a, associated with different conformations of the compounds present in solution in the two temperature regions, or (b) the presence at low-T of a dominant

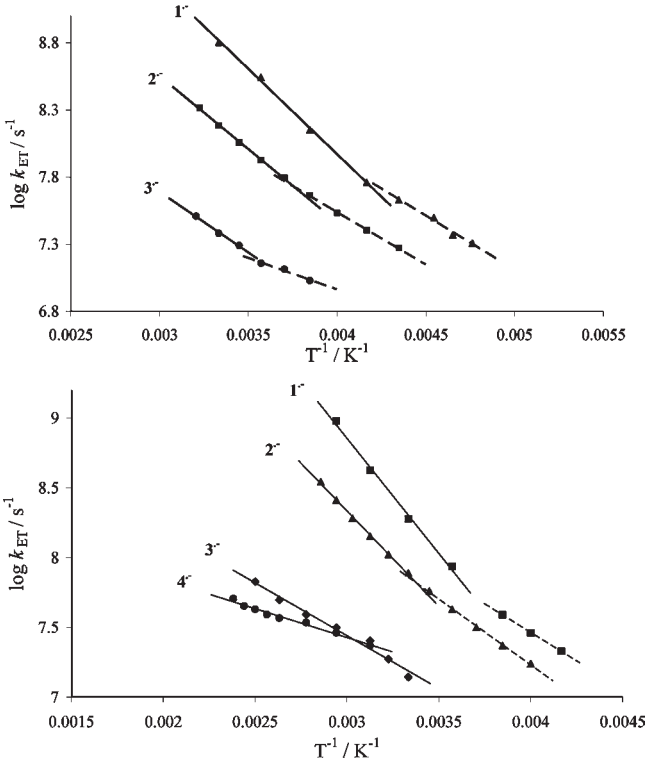

Figure 7. Top: Arrhenius plots of the IET rate constants (k_{ET}) for $\mathbf{1}^{-\bullet}$, $\mathbf{2}^{-\bullet}$, and $\mathbf{3}^{-\bullet}$ in CH_2Cl_2. Bottom: Arrhenius plots of the IET rate constants (k_{ET}) for $\mathbf{1}^{-\bullet}-\mathbf{4}^{-\bullet}$ in 1,2-dichlorobenzene. Continuous lines correspond to Arrhenius plots for high-temperature regime data, while the discontinuous lines correspond to analogous plots for the low-temperature regime data.

Table 6. Kinetic Data[a] in the Two Temperature Regions Obtained from VT-ESR Experiments for IET Processes of Mixed-Valence Species $\mathbf{1}^{-\bullet}-\mathbf{4}^{-\bullet}$ in CH_2Cl_2 and 1,2-Dichlorobenzene

T-region	parameter	$\mathbf{1}^{\bullet-}$	$\mathbf{2}^{\bullet-}$	$\mathbf{3}^{\bullet-}$	$\mathbf{4}^{\bullet-}$
			CH_2Cl_2		
high-T	A	$(1.1 \pm 0.4) \times 10^{13}$	$(6.6 \pm 1.3) \times 10^{11}$	$(2.5 \pm 1.2) \times 10^{10}$	
	E_a	5.8 ± 0.6	5.0 ± 0.3	4.1 ± 1.3	
	n; R^2	4; 0.998	5; 0.998	3; 0.995	
low-T	A	$(1.4 \pm 0.8) \times 10^{11}$	$(4.6 \pm 0.8) \times 10^{10}$	$(7.0 \pm 4.7) \times 10^{8}$	
	E_a	3.7 ± 1.1	3.6 ± 0.3	2.2 ± 1.3	
	n; R^2	4; 0.983	4; 0.999	3; 0.976	
			$C_6H_4Cl_2$		
high-T	A	$(6.4 \pm 3.8) \times 10^{13}$	$(2.7 \pm 0.6) \times 10^{12}$	$(5.1 \pm 1.6) \times 10^{9}$	$(4.7 \pm 0.6) \times 10^{8}$
	E_a	7.6 ± 1.1	6.3 ± 0.3	3.5 ± 0.5	1.9 ± 0.2
	n; R^2	4; 0.995	6; 0.998	7; 0.981	8; 0.984
low-T	A	$5.3 \pm 0.9 \times 10^{10}$	$1.0 \pm 0.2 \times 10^{11}$		
	E_a	3.7 ± 0.4	4.3 ± 0.3		
	n; R^2	3; 0.999	5; 0.998		

[a] A in s^{-1}; E_a in kcal·mol^{-1}. n is the number of temperatures used in each fitting.

dx.doi.org/10.1021/ja1083859 |J. Am. Chem. Soc. 2011, 133, 5818–5833

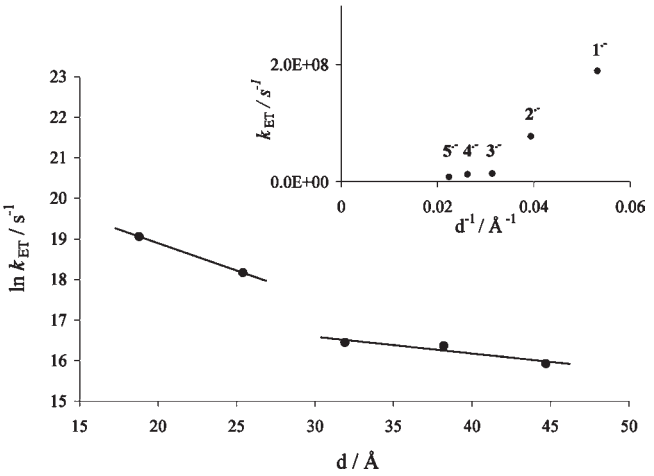

Figure 8. Dependence of the IET rate constants on the bridge lengths for $\mathbf{1}^{-\bullet}-\mathbf{5}^{-\bullet}$ in 1,2-dichlorobenzene at 300 K. Inset: Dependence of k_{ET} vs $1/d$ for such compounds.

tunneling process activated by the thermal population of specific conformations. Indeed, internal rotations may create geometries with smaller barriers to tunneling, and the process itself can appear to be temperature dependent. So, we should not neglect bridge dynamics[33] when analyzing the temperature dependence of ET, as the IET could be gated by torsional motions between the donor and the first bridge phenyl ring, as well as that occurring between the vinyl group and the phenylene linked to it.[34] Lowering the torsional barrier between the donor and the stilbenyl bridge allows more efficient electron transport between the donor and acceptor. Theoretical calculations (*vide infra*) confirmed the rich conformational space accessible for such radical anions at a relatively low energy cost.

The operative mechanism for all studied radical anions was unraveled by studying the dependence on the bridge lengths of the k_{ET} constants at one fixed temperature at which we have reliable experimental rate constants. Figure 8 depicts the plot of $\ln(k_{ET})$ versus d for $\mathbf{1}^{-\bullet}-\mathbf{5}^{-\bullet}$ in 1,2-dichlorobenzene at 300 K. In such mixed-valence molecules there appear to be two main ET regimes under these conditions. Thus, for the two shortest bridges there is a sharp decrease in the electron-transfer rate constants with the distance, similarly to that for compounds exhibiting an exponential dependence on the distance, like $k_{ET} = k_0 \exp(-\beta d)$, where IET occurs through a tunneling mechanism via superexchange.[9,10] In contrast, for the largest bridges the dependence of k_{ET} on d^{-1} points out that the IET occurs via hopping.

For the largest bridges ($\mathbf{3}^{-\bullet}-\mathbf{5}^{-\bullet}$), there is a change in mechanism regime since k_{ET} constants decrease monotonically with the length of the bridge. A fit for the two shortest bridges yields a β value of 0.140 $Å^{-1}$, which is very similar to the reported values for similar oligo-PPV bridges in other compounds,[4,9] while for the three largest bridges we obtained a value for the attenuation factor of 0.041 $Å^{-1}$. Therefore, in the shortest bridges, the contribution of the tunneling mechanism should be very significant, since the distance dependence is too abrupt to be consistent with an ET limited by hopping,[35] whereas in the longest compounds, where a very small energy gap between the PTM radical electron-acceptor unit and the PPV electron-donor bridge is anticipated (see the Absoprtion Spectra section), the preferred pathway seems to be hopping where the donor-bridge-localized states are involved. The assignment of a hopping mechanism for the longest compounds is additionally supported by the linear trend of k_{ET} versus $1/d$ observed for the largest compounds (see Figure 8 inset). This kind of transition from tunneling to hopping in long conjugated molecules has also been observed recently for wires with a different nature.[36]

As the nature of solvents may also modulate the IET rate constants of mixed-valence compounds,[37] we also decided to study such an influence using the radical anion $\mathbf{1}^{-\bullet}$. Therefore, we performed an ESR study of the thermally activated IET process of $\mathbf{1}^{-\bullet}$ in different solvents. The solvents were chosen from the 11 different classifications of the most common organic solvents, published elsewhere,[38] in order to maximize the representation of all types of solute/solvent interactions. For this solvent choice the solubility of the involved species and the electrolyte was also taken into account, as well as other solvent properties such as the dielectric constants, which should be low in order to obtain a good ESR spectra resolution, and the boiling and freezing temperatures of solvents. From all initially tested solvents, only seven had the characteristics to obtain good enough ESR spectra. The resulting VT-ESR spectra of $\mathbf{1}^{-\bullet}$ in these solvents at different temperatures, as well as the associated IET rate constants obtained by simulation of the experimental spectra, are shown in Figures S6−S10. The kinetic data obtained from Arrhenius plots of the simulated rate constants in the high-T range, where the hopping mechanism is dominant for all solvents, are given in Table S1. There are strong differences in the activation energy barriers, E_a, depending on the nature of solvents. In order to find the origin of such differences, a linear solvation energy relationship (LSER) analysis was performed with the E_a data. The LSER analysis relates the energy changes involved in a given molecular process that takes place in solution with several specific and nonspecific properties of the solvents in which the process is carried on.[39−41] The LSER model describing the E_a for $\mathbf{1}^{-\bullet}$ shows that the IET process is highly sensitive to changes of the polarity/polarizability of the solvent media (π^*) and to the hydrogen-bond donor (HBD) acidities of the solvent media (α), while other solvent parameters are unimportant (see Table S2). Thus, increasing the solvent polarity/polarizability lowers the hopping process, while increasing the HBD acidity enhances this process. This result suggests that the main interactions of solvents influencing the IET through hopping in $\mathbf{1}^{-\bullet}$ occur through the oligo-PPV bridges, where dipolar and HB interactions change, in opposite directions, the energy levels of the bridge modifying the electron hopping rates.

Theoretical Studies of Radical Anions $\mathbf{1}^{-\bullet}-\mathbf{4}^{-\bullet}$. In order to study the conformational space accessible for the studied radical anions and its influence on their electronic structures, we explored at the CASSCF/3-21G level, using various active spaces, the shape of the potential energy surface of $\mathbf{1}^{-\bullet}$. This study was made as a function of both the dihedral angles that define the coplanarity of the three central six-membered rings (two angles, ang1 and ang2, which define the coplanarity of the left and right rings of PTM units, respectively) and the most relevant distances that define the symmetric/asymmetric characteristics of the molecule. These calculations indicated that the most relevant geometric parameters defining the localization/delocalization of the electronic density were the ang1 and ang2 dihedral angles. Therefore, we decided to explore in a more systematic way the shape of the potential energy surface as a function of these two dihedral angles. These calculations were done at the ROHF/3-21G level, in order to lower the

dx.doi.org/10.1021/ja1083859 |*J. Am. Chem. Soc.* 2011, 133, 5818–5833

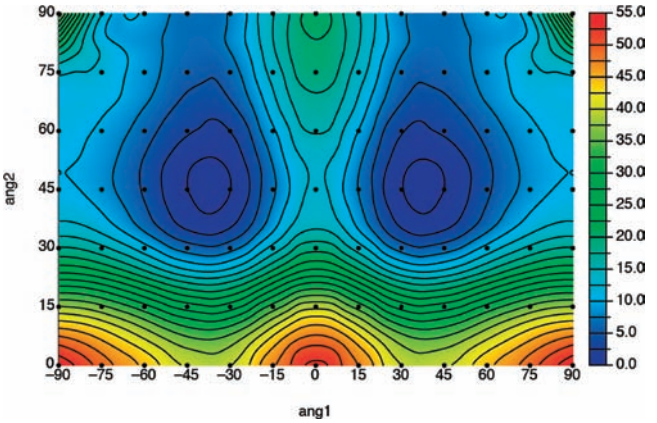

Figure 9. Shape of the potential energy surface computed for $\mathbf{1}^{-\bullet}$ as a function of the two dihedral angles that define the coplanarity of the central six-membered rings. Negative values of ang1 correspond to conrotatory movements, while positive values refer to disrotatory movements. Angles are given in degrees and energies in kcal/mol relative to the lowest energy point (placed at 38 and 45° for ang1 and ang2, respectively).

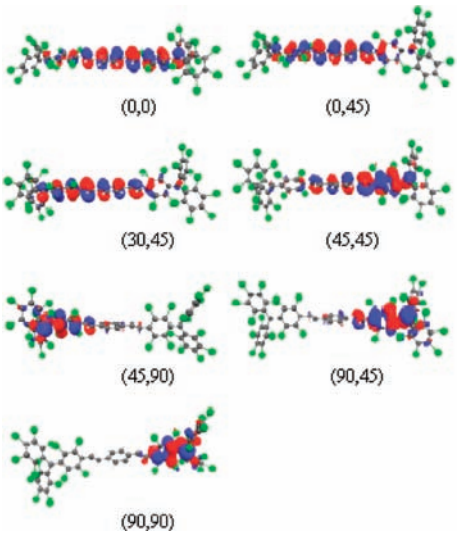

Figure 10. Shapes of the SOMO of $\mathbf{1}^{-\bullet}$ from ROHF calculations for the indicated (ang1,ang2) points. The ang1 angle corresponds to the left-side dihedral, while ang2 is for the right-side angles.

computational cost while preserving the quality of computations. For each value of ang1 and ang2, the geometry was the optimum B3LYP/3-21G geometry after changing only the dihedral angles. No further optimization was done, given the small differences in the distances found between the B3LYP and CASSCF optimum geometries.

The ROHF potential energy surface for the dihedral rotation is shown in Figure 9. The surface is almost symmetrical with respect to the 0 of the ang1 dihedral angles (the small asymmetry is due to the lack of symmetry of the B3LYP/3-21G optimum geometry, which has a C_1 symmetry). Although not plotted, it is also symmetric with respect to the 0 of the ang2 dihedral angle. The lowest energy point in this potential surface is placed at ang1 = 38° and ang2 = 45°. The three maxima at the points (ang1,ang2) = (±90, 0) and (0,0) are consequences of the steric repulsions induced by the Cl atoms when the central rings are forced to be coplanar. Other relevant points are the (±90,45) and the (±45,90) points, which correspond to the lowest energy pathways for the rotation of these dihedral angles in that potential energy surface. We also analyzed the changes in the electronic structure in the most relevant points of the potential energy surface of Figure 9. At the ROHF level, this involves simply analyzing the shape of the SOMO orbital, while at the CASSCF level one has to look into all active orbitals. In both cases we found that the most relevant change is a variation of the degree of localization/delocalization of the electronic density, which changes depending on the region of the surface evaluated. The changes detected at the ROHF level and at the CASSCF level are similar. Figure 10 plots the shape of the SOMO (in the CASSCF calculations this is selected as the orbital having an occupation closest to 1) for the characteristic points indicated before. Combining these orbital changes with Figure 10, which gives us an idea about the regions of the conformational space that can be energetically visited depending on the temperature, one can know what kind of electron localization will be observed experimentally at room temperature. At room temperature, radical $\mathbf{1}^{-\bullet}$ can thermally visit any point of the region around (±37,45), where the electron distribution is mostly located in one of the two PTM halves and the central six-membered ring. Only close to the (0,0) region is the electron distribution mostly located in the three central six-membered rings (which at this point are coplanar). However, such points are located in a high-energy region (ROHF calculations using the B3LYP geometries indicate that this region is located 55 kcal/mol above the minimum), but reoptimization of these geometries would give much smaller energy increments. The (0,0) region is the only zone of the potential energy surface where the electron distribution is symmetrically located in the central three six-membered rings.

As complementary information, we also computed the relative energy and electronic structure of the first excited state at points (45,45), (0,45), and (45,90). The calculations were done at the CASSCF(7,7)/3-21G level. The first excited state is located between 33 and 36 kcal/mol above the ground state for the same point, depending on the angles. The electronic distribution is symmetrical and highly delocalized over the central part of the molecule. Thus, this is a surface that will be accessible photochemically, but not thermally, being responsible for the optically induced IVT (*vide supra*).

We also computed the effect of increasing the number of PPV units that connect the two PTM units. The SOMO shapes calculated at the ROHF/3-21G level for the (45,45) point for radical anions $\mathbf{2}^{-\bullet}$ and $\mathbf{3}^{-\bullet}$ exhibit an asymmetry (see Figure S12), as also occurs for $\mathbf{1}^{-\bullet}$ (see Figure 10). For radical anion $\mathbf{4}^{-\bullet}$, the electronic distribution is found to be symmetrically delocalized over the central six-membered rings. A more detailed investigation of all studied radical anions, taking into account the presence of solvents, is required for a more quantitative evaluation of the trends, as has been observed for other mixed-valence systems.[41] Nevertheless, the overall trend is that the symmetric delocalized state becomes more stable as the number of PPV units is increased.

CONCLUSIONS

Conjugated diradicals **1**−**5** with different lengths, incorporating from one to five PPV units between two polychlorinated triphenylmethyl (PTM) radical units, have been prepared using

Wittig−Horner-type chemistry. Chemical and electrochemical reduction of the diradicals **1**−**5** gave the series of radical anions $\mathbf{1}^{-\bullet}$−$\mathbf{5}^{-\bullet}$ and dianions $\mathbf{1}^{2-}$−$\mathbf{5}^{2-}$, which were fully characterized. To the best of our knowledge, radical anions $\mathbf{1}^{-\bullet}$−$\mathbf{5}^{-\bullet}$ enabled to study for the first time, by means of UV−vis−NIR and ESR spectroscopies, the long-range IET phenomena in the ground state in a series of mixed-valence species with increasing lengths and without using any external perturbation. The temperature dependence of the IET rate constants of mixed-valence species $\mathbf{1}^{-\bullet}$−$\mathbf{5}^{-\bullet}$ revealed the presence of two different regimes at low and high temperatures. In each of these regimes a different IET mechanism dominates. Thus, at higher temperatures the dominant mechanism is the thermally activated hopping one, while at low temperatures electron tunneling via superexchange is the operative mechanism. Both mechanisms occur to different extents depending on the length of the mixed-valence compounds. Thus, the lengths of the oligo-PPV bridges have a notable influence on the activation energy barriers of the hopping processes, diminishing the barriers as the lengths are increased. The nature of solvent also modifies the IET rates when they are controlled by the hopping mechanism by means of the interactions between the PPV bridges and the solvents. In the shortest compounds $\mathbf{1}^{-\bullet}$ and $\mathbf{2}^{-\bullet}$, optically induced IET through a superexchange mechanism was also observed, both mixed-valence species exhibiting intervalence bands whose intensities decreased with the length of the PPV fragment as the electronic coupling between the PTM units does.

EXPERIMENTAL SECTION

General Procedures. All reactions were carried out under Ar and using solvents which were dried carefully by routine procedures. For column chromatography, silica gel 60 (230−400 mesh, 0.040−0.063 mm) was purchased from E. Merck. Thin-layer chromatography (TLC) was performed on glass sheets coated with silica gel 60 F_{254} purchased from E. Merck, visualized by UV light. NMR spectra were recorded on a Bruker AC 200 (200 MHz) or a Bruker AM 400 (400 MHz) instrument with solvent peaks as reference. Mass measurements were carried out on a Bruker BIFLEX matrix-assisted laser desorption/ionization time-of-flight (MALDI-TOF) mass spectrometer. A saturated solution of 1,8,9-trihydroxyanthracene (dithranol, Aldrich, EC 214-538-0) in CH_2Cl_2 was used as a matrix. For diradicals **1**−**5** and monoaldehydes **6**−**10**, no matrix was used, or in some cases nitroanthracene. FAB mass spectra were obtained on a VG AutoSpec instrument, using *m*-nitrobenzyl alcohol as a matrix. FT-IR spectra were recorded on a Nicolet Impact 410 spectrophotometer using KBr disks. Elemental analyses were performed by the analytical service at the Institut Charles Sadron, Strasbourg, and in the Servei d'Anàlisi Química de la UAB. UV−vis−near-IR spectra were taken on a Varian Cary 5 E spectrophotometer. ESR spectra were obtained on an X-band spectrometer (Bruker ESP 300 E) equipped with a field-frequency (F/F) lock accessory and built-in NMR gaussmeter. A rectangular TE102 cavity was used for the measurements. The signal-to-noise ratio of spectra was increased by accumulation of scans using the F/F lock accessory to guarantee large field reproducibility. Precautions to avoid undesirable spectral distortions and line broadenings, such as those arising from microwave power saturation and magnetic field overmodulation, were also taken. To avoid dipolar line broadening from dissolved oxygen, solutions were always carefully degassed with pure argon. The CV measurements were performed on an EG&G PAR 263A potentiostat/galvanostat controlled by a personal computer and driven by dedicated software. CV was performed with a conventional three-electrode configuration consisting of platinum working and auxiliary electrodes and a $Ag/AgNO_3$ reference electrode. The experiments were carried out in dry CH_2Cl_2 containing 0.1 M $[(n\text{-}Bu)_4N]PF_6$ as supporting electrolyte. Deoxygenation of the solutions was achieved by bubbling argon for at least 5 min, and the working electrode was cleaned after each run. The cyclic voltammograms were recorded with a scan rate increasing from 0.05 to 1.00 V s^{-1}. Ferrocene was used as an internal reference for calibrating the redox potentials and checking the reversibility of the electrochemical setup. The theoretical redox potential for $FeCp_2$ vs Ag^+/Ag in CH_2Cl_2 was assumed to be 0.46 V.[42]

Synthesis of Compounds. Compounds **6**, **8**, **10**, **16**, and **17** were prepared according to previously reported procedures,[17] while the preparation of compounds **1**−**5** and **18** is given in the Supporting Information.

Theoretical Calculations. B3LYP and CASSCF calculations were done using the appropriate options in the Guassian03 program.[43] The B3LYP functional is the three-parameter functional of Becke, a hybrid functional that mixes Hartree−Fock exchange with the Lee−Yang−Parr exchange-correlation functional (a class of gradient-corrected exchange and correlation functionals). The CASSCF(*n*,*m*) calculations (complete active space multiconfiguration self-consistent field computation on (*n*,*m*) active space) were obatined by combining the *n* electrons and the *m* orbitals of the active space in all possible forms.[44] The smallest active space selected in this study was the (3,3) active space, obtained by selecting the SOMO, SOMO−1, and LUMO orbitals in a UB3LYP computation. The remaining active spaces were obtained by increasing the number of electrons and orbitals in an appropriate way, the largest one being a (7,7) active space. With this active space we confirmed the validity of the computations done with smaller active spaces. Geometry optimizations were done using the usual procedures within Gaussian; in the B3LYP and CASSCF cases all analytical gradients were used. The minimum condition in full minimizations was confirmed by looking at the vibrational frequencies.

ASSOCIATED CONTENT

Supporting Information. Complete refs 1 and 43; synthesis of compounds **6**, **8**, **10**, **16**, and **17**; comparative UV−vis spectra of **2**, **7**, and **11**; VT-ESR spectra of radical anions $\mathbf{1}^{-\bullet}$ and $\mathbf{3}^{-\bullet}$ in CH_2Cl_2; VT-ESR spectra of radical anions $\mathbf{1}^{-\bullet}$ and $\mathbf{3}^{-\bullet}$ in 1,2-dichlorobenzene; VT-ESR spectra of radical anions $\mathbf{1}^{-\bullet}$ −$\mathbf{3}^{-\bullet}$ and $\mathbf{5}^{-\bullet}$ in 1,2-dichlorobenzene; ESR spectra at 300 K of radical anions $\mathbf{1}^{-\bullet}$−$\mathbf{5}^{-\bullet}$ in 1,2-dichlorobenzene; VT-ESR spectra of radical anion $\mathbf{1}^{-\bullet}$ in anisole, ethyl acetate, toluene, chloroform, and benzonitrile; theoretical calculations of the conformational space and the electronic structure of radical anions $\mathbf{1}^{-\bullet}$−$\mathbf{4}^{-\bullet}$; and a detailed study of the influence of solvents on IET of radical anion $\mathbf{1}^{-\bullet}$ by the linear solvation energy relationship. This material is available free of charge via the Internet at http://pubs.acs.org.

AUTHOR INFORMATION

Corresponding Author
vecianaj@icmab.es; cun@icmab.es

ACKNOWLEDGMENT

The authors thank EU Large Project ONE-P (FP7-NMP-2007-212311), Instituto de Salud Carlos III through "Acciones CIBER", the MICINN, Spain (CTQ2006-06333/BQU and CTQ2010-19501/BQU), and Generalitat de Catalunya (2009SGR158). The team from Universitat de Barcelona thanks the

MICINN Spanish (MAT2008-02032/MAT-FEDER Fonds co-financed, and UNBA05-33-001) for support and CESCA and BSC for computer time.

REFERENCES

(1) Adams, D. M.; et al. *J. Phys. Chem. B* **2003**, *107*, 6668.

(2) Marcus, R. A.; Sutin, N. *Biochim. Biophys. Acta* **1985**, *811*, 265.

(3) Isied, S. S.; Ogawa, M. Y.; Wishart, J. F. *Chem. Rev.* **1992**, *92*, 381.

(4) (a) *Electron Transfer in Chemistry*; Balzani, V., Ed.; Wiley: Weinheim, 2001; Vols. I–V. (b) Fox, M. A., Ed. *Chem. Rev.* **1992**, *92*, 365–490. (c) Paddon-Row, M. N. *Acc. Chem. Res.* **1994**, *27*, 18. (d) Schab, P. F. H.; Levin, M. D.; Michl, J. *Chem. Rev.* **1999**, *99*, 1863. (e) Segal, D.; Nitzan, A.; Davis, W. B.; Wasielewski, M. R.; Ratner, M. A. *J. Phys. Chem. B* **2000**, *104*, 3817. (f) Giese, B. *Acc. Chem. Res.* **2000**, *33*, 631. (g) Launay, J. P. *Chem. Soc. Rev.* **2001**, *30*, 386. (h) Giese, B.; Amaudrut, J.; Kohler, A. K.; Spormann, M.; Wessely, S. *Nature* **2001**, *412*, 318. (i) Wold, D. J.; Haag, R.; Rampi, M. A.; Frisbie, C. D. *J. Phys. Chem. B* **2002**, *106*, 2813. (j) Nakamura, T.; Fujitsuka, M.; Araki, Y.; Ito, O.; Ikemoto, J.; Takimiya, K.; Aso, Y.; Otsubo, T. *J. Phys. Chem. B* **2004**, *108*, 10700. (k) Engelkes, V. B.; Beebe, J. M.; Frisbie, C. D. *J. Am. Chem. Soc.* **2004**, *126*, 14287. (l) Conwell, E. M. *Proc. Natl. Acad. Sci. U.S.A.* **2005**, *102*, 8795. (m) Choi, S. H.; Kim, B.; Frisbie, C. D. *Science* **2008**, *320*, 1482. (n) Lu, Q.; Liu, K.; Zhang, H.; Du, Z.; Wang, X.; Wang, F. *ACS Nano* **2009**, *3*, 3861.

(5) Ratner, M. A.; Jortner, J. In *Molecular Electronics*; Jortner, J., Ratner, M., Eds.; Blackwell: Oxford, 1997; p 5.

(6) Davis, W. B.; Wasielewski, M. R.; Ratner, M. A.; Mujica, V.; Nitzan, A. *J. Phys. Chem. A* **1997**, *101*, 6158.

(7) Okada, A.; Chernyak, V.; Mukamel, S. *J. Phys. Chem. A* **1998**, *102*, 1241.

(8) Pollard, W. T.; Felts, A. K.; Friesner, R. A. *Adv. Chem. Phys.* **1996**, *93*, 77.

(9) (a) Helms, A.; Heiler, D.; McLendon, G. *J. Am. Chem. Soc.* **1992**, *114*, 6227. (b) Davis, W. B.; Svec, W. A.; Ratner, M. A.; Wasielewski, M. R. *Nature* **1998**, *396*, 60. (c) Davis, W. B.; Ratner, M. A.; Wasielewski *J. Am. Chem. Soc.* **2001**, *123*, 7877. (d) Giacalone, F.; Segura, J. L.; Martín, N.; Guldi, D. M. *J. Am. Chem. Soc.* **2004**, *126*, 5340. (e) Giacalone, F.; Segura, J. L.; Martín, N.; Raney, J.; Guldi, D. M. *Chem.—Eur. J.* **2005**, *11*, 4819. (f) Lancaster, K.; Odom, S. A.; Jones, S. C.; Thayumanavan, S.; Marder, S. R.; Brédas, J.-L.; Coropceanu, V.; Barlow, S. *J. Am. Chem. Soc.* **2009**, *131*, 1717.

(10) (a) Weiss, E. A.; Ahrens, M. J.; Sinks, L. E.; Gusev, A. V.; Ratner, M. A.; Wasielewski, M. R. *J. Am. Chem. Soc.* **2004**, *126*, 5577. (b) Malak, R. A.; Gao, Z.; Wishart, J. F.; Isied, S. S. *J. Am. Chem. Soc.* **2004**, *126*, 13888.

(11) Goldsmith, R. H.; Sinks, L. E.; Kelley, R. F.; Betzen, L. J.; Liu, W.; Weiss, E. A.; Ratner, M. A.; Wasielewski, M. R. *Proc. Natl. Acad. Sci. U.S.A.* **2005**, *102*, 3540.

(12) Paddon-Row, M. N. In *Electron Transfer in Chemistry*; Balzani, V., Ed.; Wiley-VCH: Weinheim, 2001; Vol. III, Part 2, p 179.

(13) (a) Bonvoisin, J.; Launay, J.-P.; Rovira, C.; Veciana, J. *Angew. Chem., Int. Ed. Engl.* **1994**, *33*, 2106. (b) Sedo, J.; Ruiz, D.; Vidal-Gancedo, J.; Rovira, C.; Bonvoisin, J.; Launay, J.-P.; Veciana, J. *Adv. Mater.* **1996**, *8*, 748. (c) Rovira, C.; Ruiz-Molina, D.; Elsner, O.; Vidal-Gancedo, J.; Bonvoisin, J.; Launay, J.-P.; Veciana, J. *Chem.—Eur. J.* **2001**, *7*, 240. (d) Elsner, O.; Ruiz-Molina, D.; Vidal-Gancedo, J.; Rovira, C.; Veciana, J. *Nano Lett.* **2001**, *1*, 117.

(14) (a) Ballester, M. *Acc. Chem. Res.* **1985**, *297*, 131. (b) Veciana, J.; Riera, J.; Castañer, J.; Ferrer, N. *J. Organomet. Chem.* **1985**, *297*, 131. (c) Armet, O.; Veciana, J.; Rovira, C.; Riera, J.; Castañer, J.; Molins, E.; Rius, J.; Miravitlles, C.; Olivella, S.; Brichfeus, J. *J. Phys. Chem.* **1987**, *91*, 5608.

(15) (a) Smart, J. C.; Pinsky, B. L. *J. Am. Chem. Soc.* **1980**, *103*, 1009. (b) Kramer, J. A.; Hendrickson, D. N. *Inorg. Chem.* **1980**, *19*, 3330.

(16) (a) Rak, S. F.; Miller, L. L. *J. Am. Chem. Soc.* **1992**, *114*, 1388. (b) Nelsen, S. F.; Ismagilov, R. F.; Trieber, D. A., II *Science* **1997**, *278*, 846. (c) Lindeman, S. V.; Rosokha, S. V.; Sun, D.; Kochi, J. K. *J. Am. Chem. Soc.* **2002**, *124*, 843. (d) Gautier, N.; Dumur, F.; Lloveras, V.; Vidal-Gancedo, J.; Veciana, J.; Rovira, C.; Hudhomme, P. *Angew. Chem., Int. Ed.* **2003**, *42*, 2765.

(17) Langa, F.; Gomez-Escalonilla, M. J.; Rueff, J.-M.; Figueira-Duarte, T. M.; Nierengarten, J.-F.; Palermo, V.; Samor, P.; Rio, Y.; Accorsi, G.; Armaroli, N. *Chem.—Eur. J.* **2005**, *11*, 4405.

(18) Müllen, K.; Wegner, G. *Electronic Materials: the Oligomer Approach*, Wiley-VCH: Weinheim, 1998.

(19) House, H. O. *Modern Synthetic Reactions*, 2nd ed.; Benjamin: Menlo Park, CA, 1972; p 608.

(20) (a) Wurst, K.; Elsner, O.; Schottenberger, H. *Synlett* **1995**, 833. (b) Rodríguez, J.-G.; Oñate, A.; Martin-Villamil, R. M.; Fonseca, I. *J. Organomet. Chem.* **1996**, *513*, 71.

(21) Fitjer, L.; Quabeck, U. *Synth. Commun.* **1985**, *15*, 855.

(22) Peeters, E.; van Hal, P. A.; Knol, J.; Brabec, C. J.; Sariciftci, N. S.; Hummelen, J. C.; Janssen, R. A. J. *J. Phys. Chem. B* **2000**, *104*, 10174.

(23) Armaroli, N.; Accorsi, G.; Gisselbrecht, J. P.; Gross, M.; Krasnikov, V.; Tsamouras, D.; Hadziioannou, G.; Gomez-Escalonilla, M. J.; Langa, F.; Eckert, J. F.; Nierengarten, J.-F. *J. Mater. Chem.* **2002**, *12*, 2077.

(24) Ballester, M.; Riera, J.; Castañer, J.; Rodriguez, A.; Rovira, C.; Veciana, J. *J. Org. Chem.* **1982**, *47*, 4498.

(25) *Electronic Paramagnetic Resonance*; Weil, J. A., Bolton, J. R., Eds.; Wiley and Sons: New York, 1994.

(26) Lloveras, V.; Vidal-Gancedo, J.; Ruiz-Molina, D.; Figueira-Duarte, T. M.; Nierengarten, J.-F.; Veciana, J.; Rovira, C. *Faraday Discuss.* **2006**, *131*, 291.

(27) Dumur, F.; Gautier, N.; Gallego-Planas, N.; Sahin, Y.; Levillain, E.; Mercier, N.; Hudhomme, P.; Masino, M.; Girlando, A.; Lloveras, V.; Vidal-Gancedo, J.; Veciana, J.; Rovira, C. *J. Org. Chem.* **2004**, *69*, 2164.

(28) Robin, M.; Day, P. *Adv. Inorg. Radiochem.* **1967**, *10*, 247.

(29) It is well known that the unpaired electron of highly chlorinated triphenylmethyl radicals and the negative charge of their corresponding carbanions are mainly localized on the α carbons.[14] Therefore, the two α carbon atoms of the radical anions $\mathbf{1}^{-\bullet}$–$\mathbf{5}^{-\bullet}$ can be considered in a first approximation as the electron active sites for the ET phenomena. It must also be noticed that, as far as IET phenomena are concerned, the main distance to be considered is the through-bond distance between the two electron active sites; i.e., the sum of bond lengths corresponding to the conjugated pathway. However, as shown by ESR, the average distance between the two spins—the average interspin separation—differs from the nominal separation, either through-space or through-bond, between the two radical α carbon atoms obtained from the AM1-minimized structures, due to the different extents of delocalization in both diradicals.

(30) McCreery, R. L. *Chem. Mater.* **2004**, *16*, 4477.

(31) Hush, N. S. *Coord. Chem. Rev.* **1985**, *64*, 135.

(32) (a) Heinzer, J. *J. Mol. Phys.* **1971**, *22*, 167. (b) Heinzer, J. *Quantum Chemistry Program Exchange* **1972**, No. 209.

(33) (a) Petterson, K.; Kyrychenko, A.; Rönnow, E.; Ljungdahl, T.; Martensson, J.; Albinsson, B. *J. Phys. Chem. A* **2006**, *110*, 310. (b) Eng, M. P.; Ldungdahl, T.; Martensson, J.; Albinsson, B. *J. Phys. Chem. B* **2006**, *110*, 6483. (c) Scott, A. M.; Ricks, A. B.; Calvin, M. T.; Wasieleski, M. R. *Angew. Chem., Int. Ed.* **2010**, *49*, 2904.

(34) Davis, W. B.; Ratner, M. A.; Wasielewski, M. R. *J. Am. Chem. Soc.* **2001**, *123*, 7877.

(35) Sikes, H. D.; Smalley, J. F.; Dudek, S. P.; Cook, A. R.; Newton, M. D.; Chidsey, C. E. D.; Feldberg, S. W. *Science* **2001**, *291*, 1519.

(36) (a) Choi, S. H.; Risko, C.; Ruiz-Delgado, M. C.; Kim, B.; Brédas, J.-L.; Frisbe, C. D. *J. Am. Chem. Soc.* **2010**, *132*, 4358. (b) Hines, T.; Diez-Perez, I.; Hihath, J.; Liu, H.; Wang, Z.-S.; Zhao, J.; Zhou, G.; Müllen, K.; Tao, N. *J. Am. Chem. Soc.* **2010**, *132*, 11658.

(37) Nielsen, S. F.; Trieber, D. A.; Ismagilov, R. F.; Teki, Y. *J. Am. Chem. Soc.* **2001**, *123*, 5684.

(38) Ventosa, N.; Ruiz-Molina, D.; Sedo, J.; Rovira, C.; Tomas, X.; Andre, J.-J.; Bieber, A.; Veciana, J. *Chem.—Eur. J.* **1999**, *5*, 3533.

(39) Taft, R. W.; Abboud, J. L. M.; Kamlet, M. J.; Abraham, M. H. *J. Solution Chem.* **1985**, *14*, 153.

(40) Kamlet, M. J.; Taft, R. W. *J. Chem. Soc., Perkin Trans.* **1979**, *2*, 337.

(41) Kamlet, M. J.; Doherty, R. M.; Carr, P. W.; Mackay, D.; Abraham, M. H.; Taft, R. W. *Environ. Sci. Technol.* **1988**, *22*, 503.
(42) Connelly, N. G.; Geiger, W. E. *Chem. Rev.* **1996**, *96*, 877–910.
(43) Frisch, M. J.; et al. *Gaussian03*, Revision C.02; Gaussian, Inc.: Wallingford, CT, 2004.
(44) Hegarty, D.; Robb, M. A. *Mol. Phys.* **1979**, *38*, 1795.